Operando Spectro-electrochemical investigations of Pt and Pt-alloys as fuel cell catalysts

Nagra, H.J.

A Supplementary Information for Chapter 2

A Supplementary Information on Chapter 2

A2.1 Manipulator and Load lock Design

The manipulator design was made with three scenarios in mind: i) Ex-situ investigation of solid state samples in vacuum, ii) In situ investigation of electrochemical reactions and iii) In situ investigation of gas-solid reactions and interfaces at higher temperatures (under development). The first two scenarios are addressed using interchangeable extensions that can be fitted on the same manipulator platform, circumventing the need to design and construct separate manipulators for each purpose and thus greatly reducing the complexity of the setup. The primary application of the set-up is electrochemistry including fundamental studies on the electric double layer structure in electrochemical systems and effects of different ions in electrochemical reactions [1], cathodic corrosion of precious metal catalysts[2], and more applied research areas such as fuel cell degradation, energy storage and battery systems[3], all of which require very different experimental conditions.

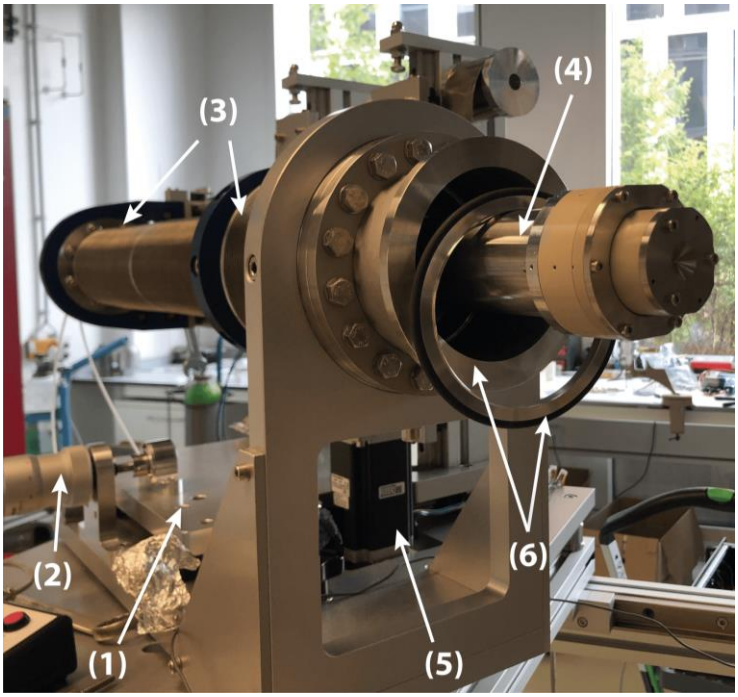

Figure A2.1 : External overview of manipulator assembly and the electrochemical cell and the manipulator shows the state before the cell is placed in the system. The axial movement of the cell is managed by an electronic drive unit for precise position, while the horizontal and vertical positions can be adjusted by micrometer screws

Figure A2.1 shows the manipulator assembly, where the manipulator is mounted on a rotation table (1) which is capable of rotating 45° to allow convenient sample exchange. The assembly is also fitted with micrometer screws to manually adjust the positioning of the sample in the X,Y and Z planes (2). The manipulator (3) consists of two annular tubes; the outer tube consists of two sections of expandable bellows supported by the manipulator manifold on which it is mounted, while the inner tube is a standard 316L stainless steel tube on which the electrochemical cell is mounted. The electrolyte supply lines, safety valves and potentiostat

wires connected to the cell run through the inside of the tube which is not part of the vacuum, so that standard components used in electrochemical labs can be employed without risk of vacuum contamination. The manipulator is fitted with step motors (5) and operated by an electronic console to move/ retract the sample into/out of the main chamber. The manipulator is connected to the sample preparation chamber (load lock) via an ISO flange (6), which can be opened quickly to facilitate rapid sample exchange. Once the sample is secured inside the load lock, it is pumped down via a scroll pump to ~10^{-2} mbar before introducing the cell into the main chamber.

A2.2 Main Chamber

The main chamber of the setup is a spherical chamber made of 316L Austenitic stainless steel and is connected to the load lock via a gate valve (VAT Vakuumventile AG). This gate valve isolates the main chamber from the load lock during sample exchange and leak testing of the electrochemical cell. The chamber has a central window for a clear view and maintenance access. Figure2.1 in the main text also shows a UHV chamber connected to the main chamber and is pumped by a large turbomolecular pump (Pfeiffer Vacuum HiPace 700). The UHV chamber is separated from the main chamber by a pneumatically operated butterfly valve (VAT Vakuumventile AG) which is kept open during the ex-situ measurements to maintain a lower pressure in the main chamber and kept closed during NAP-XPS measurements. The main chamber is fitted with two capacitive pressure gauges to cover the pressure range from ambient pressure up to 10^{-5} mbar. In order to shield the samples from the stray magnetic fields due to the electrical equipment around the setup, 3 pairs of Helmholtz coils are installed around the main chamber to counteract the in X,Y and Z directions. A measured current is run through these coils that generates a counter magnetic field, so that the resultant magnetic field strength inside the chamber is zero.

Additional features consist of a sputter gun (IS 40C1, PREVAC), a leak valve (VAT Vakuumventile AG) to dose gases into the main chamber, a PREVAC LED lighting system, and a high-resolution camera for sample alignment (Baumer Optronics GmbH).

A2.3 X-ray Source and Analyzer

The setup has a SPECS Al Kα lab x-ray source (µFOCUS 600 Monochromated X-ray Source, E= 1486.7 eV) which produces high intensity X-rays with a spot size under 200 µm on the sample. The small spot size permits a monochromator resolution of 0.25 eV to be achieved for Al Kα. The lab source is equipped with a near ambient pressure (NAP) extension containing a SiN_x window that separates the X-ray source chamber from the main chamber, enabling measurements at pressures as high as ~25 mbar, while maintaining high vacuum in the X-ray source chamber. The X-ray source is cooled by cooling water supplied through a control unit (SPECS CCX70 Control Unit) designed to provide high voltage isolation, controlled water pressure and temperature as well as filtering against particulate matter.

The analyzer unit is SPECS PHOIBOS 150, which contains a 3-stage differential pumping system with tunable apertures and a 1-D delay line detector (DLD). A pneumatic gate valve separates the pre-lens system from the rest of the analyzer in case a high pressure is detected in the

main chamber, which will be discussed in detail in the interlock section of the paper. The analyzer is interface with the main chamber through a 300 µm aperture nozzle. The apertures and pumping speed of the analyzer is tuned such that measurements up to 25 mbar can be performed. In order to keep track of the gaseous products formed during the heterogeneous reactions as well as water and other vapors escaping during electrochemical reactions during in situ XPS experiments, an online quadrupole mass analyzer (RGA 200, Stanford Research Instruments) is placed between the first and the second differential pumping stage. Gases and vapors escaping the main chamber into the analyzer unit are detected and analyzed inline in real time, giving information about the composition of the gaseous mixture at the sample surface.

A2.4 Electrolyte and Gas Supply

The electrochemical manipulator extension is connected to an electrolyte supply system capable of switching between different electrolytes. This is made possible by installing several electrolyte bottles to the same supply and return electrolyte lines with a selection valve in between. The selection valves used in this case enable up to four electrolyte bottles to be connected to the system, enabling a closed circulation by setting the supply and return selection valves to the same bottle. It is also possible to bubble a selection of gases through the electrolyte depending on the requirement of the reaction. Figure A2.2 shows the schematic diagram of the electrolyte supply system.

One of the most frequent problems encountered in in situ electrochemical spectroscopy is the air bubble entrapment at the electrodes. This disrupts the electrolyte connection between the electrodes and causes high solution resistance and noise in the voltametric readings. In order to solve this problem, we have installed a vacuum pumped bubble trap (Darwin Microfluidics) which removes any bubbles and undissolved gases from the electrolyte before it reaches the cell.

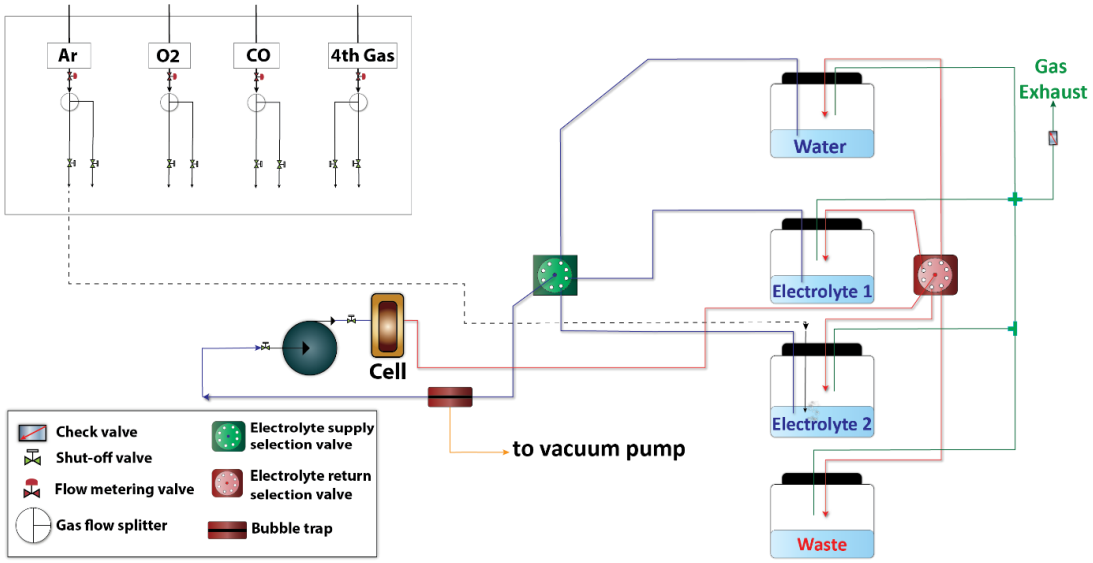

Figure A2.2 : Schematic diagram of the electrolyte and gas supply

A2.5 Safety Interlock System

A number of safety features are installed in the system to safeguard it in case of a variety of adverse scenarios. The idea behind designing the safety interlock system is to a) preserve the main chamber vacuum, b) prevent electrolyte leakage into the main chamber, c) protect the analyzer against the liquid droplets and d) protect the x-ray source and NAP extension window against liquid spillage and abrupt changes in pressure. Most of these securities become relevant while the electrochemical flow cell is in operation due to the risks associated with operating a liquid flow cell in a vacuum chamber. The safety systems can be broadly classified as *pressure safety system* and *power failure safety system*, which are briefly described as below and are shown as a schematic in Figure A2.3:

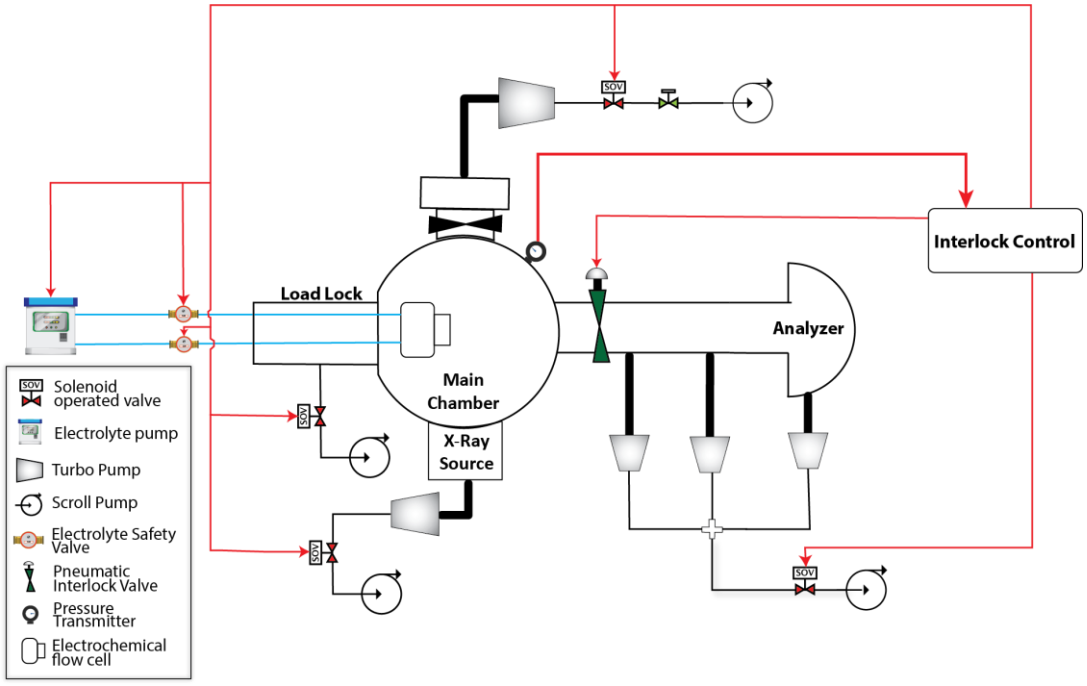

Figure A2.3 : Safety Interlock Schematic for EC-NAP-XPS

i) Pressure Safety Interlock

As mentioned earlier, there is a risk of electrolyte spillage from the flow cell into the vacuum. This can, in addition to spillage of (sometimes corrosive) electrolyte into the main chamber, result in electrolyte droplets being sucked into the high voltage parts of the analyzer and the X-ray source. In order to minimize the risk in case of leakage from the electrochemical cell, the pressure safety interlock is programmed to detect abrupt rises in pressure inside the main chamber. In case of detection of a pressure rise due to an electrolyte leak, the pressure transmitter coupled with the interlock control will trigger the emergency steps. These emergency steps include stopping the electrolyte pump, closing the safety valves on the electrolyte supply/return lines and closing the pneumatic interlock valve on the pre-lens stage of the analyzer system.

ii) Power Failure Interlock

The power failure interlock is aimed at preserving a static vacuum inside the setup in case of a power failure. In case of a power failure, the system can vent rapidly resulting in rupturing of the SiN_x window installed in the X-ray source NAP extension as well damage to the turbo pumps. To prevent that, the interlock is programmed to close all the solenoid operated valves (SOVs) installed between the turbo and scroll pumps immediately.

A2.6 Bake out

The entire setup can be baked out partially or all at once. In partial bake-out, the setup is divided into separate temperature zones, which makes it is possible to separately bake-out the analyzer, main chamber and the x-ray source using a combination of PREVAC BCU14 and Hemi Heating bakeout controllers.

A2.7 Cleaning procedure for components that are wetted in electrochemical experiments

Trace impurities present in the electrolyte can cause diminishing of the charge of existing voltametric measurements as well as introduce erroneous peaks[4] rendering the results unreliable.

To be able to produce reliable electrochemistry, all the surfaces of the electrochemical setup that come in contact with the electrolyte can be cleaned to glass cell electrochemistry standards. An acidified solution $KMnO_4$ at pH 1 was prepared in one of the electrolyte bottles and circulated through the electrochemical cell for several hours on circulation. $KMnO_4$ is a strong oxidizing agent and removes the adsorbed impurities on the surfaces. The circulating solution was replaced with a 10% solution of H_2SO_4 and H_2O_2 (piranha solution) in ultra-high purity water (MiliQ, 18.2 MΩ.cm) followed by warm MiliQ water to rinse. The materials of construction for the electrochemical setup have been chosen such they are highly stable against harsh pH conditions[5].

A2.8 Curve fitting parameters for Pt 4f

The raw XPS data was processed using CasaXPS Version 2.3.23. A Shirley background subtraction was used for all the datasets. The Lorentzian LF line shape was employed, which is an extension of Lorentzian LA line shape, the purpose of which is to limit the intensity of the asymmetric tails. It fits the data on the basis of 4 parameters;α, β, w and m. Varying 'α' and 'β' results in increasing or decreasing the spread of the tail for the Lorentzian curve, thereby affecting how steep are the edges of the line shape. 'm' is the integer specifying the Lorentzian convolution by the gaussian function and 'w' is the dampening factor to force the tails of the curve to reduce towards the limits of integration. An asymmetric form of Lorentzian LF line shape function was used for fitting the raw Pt 4f spectra. It is known through literature that, as a consequence of spin-orbit coupling, the electrons that leave Pt 4f orbital, generate two distinct energy peaks in the XPS spectrum categorized as $4f_{5/2}$ and $4f_{7/2}$. Hence doublets for Pt^0 $Pt^{\delta+}$, Pt^{2+} and Pt^{4+} were used, with a constant spin-orbit splitting of 3.34 eV and a peak area

ratio of 3:4 for the $4f_{5/2}$ and $4f_{7/2}$ peaks. The details of the fitting parameters are shown in the table below.

The ranges for the peak positions of different Pt oxidation states were determined in accordance with the literature, especially cited in detail by Savelena and their group[6] and previous work[7]. In order to accommodate the variations in the configuration of the beam energy for different experiments, a slight variation in the binding energy for Pt^0 (± 0.1 eV) was permitted. The line shape parameters were determined by comparing to the *ex-situ* XPS spectrum of a clean Pt foil to accommodate for the properties of the lab X-ray source. The Pt^{4+} line shape, peak position, and FWHM were determined by free fitting of a highly oxidized 3nm Pt sample produced at 1.5 V_{RHE}, which displays a well-resolved Pt^{4+} peak. The line shape and FWHM of the other components was determined at low potential, where the metallic contribution is dominant. Note, however, that there is no potential at which only one component could be fitted. This is in line with the notion that the Pt surface atom are always in contact with adsorbates (e.g. H_2O, OH, O, R-SO_3^-), which generates a $Pt^{\delta+}$ and a bulk Pt^0 peak. The consistency of the fit model was ensured by applying it to several data sets.

	Pt^0	**$Pt^{\delta+}$**	**Pt^{2+}**	**Pt^{4+}**
Line shape	LF(0.63,2,20,50)	LF(0.63,2,20,50)	LF(0.63,2,20,50)	LF(1.8,2,10,0)
Peak Position	71.1 - 70.9	72 - 71.2	72.7 - 72	Determined at highest potential of the dataset
FWHM	Free	Same as Pt^0	Same as Pt^0	Determined at highest potential of the dataset

Table A1.1 : Fitting parameters for Pt 4f spectral decomposition

A2.9 SEM Images of Graphene on membrane electrode assembly

As mentioned in the main text, low magnification images show a clear contrast between graphene covered and uncovered parts of the MEA.

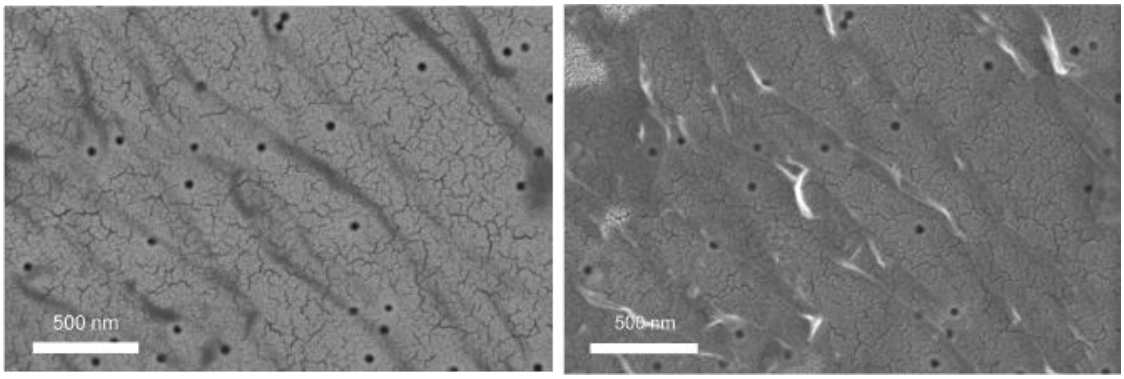

Figure A2.4 :Images of the 'pristine' film which show clearly the graphene layer on top of the Membrane Electrode Assembly

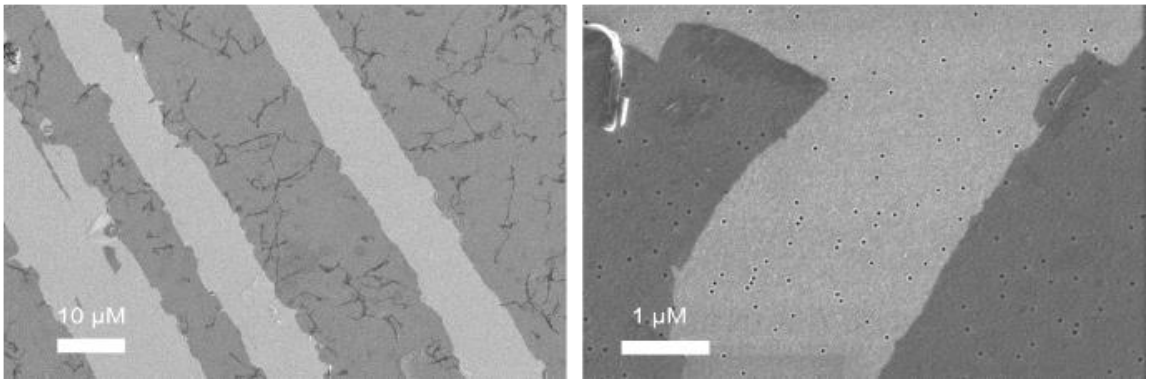

Figure A2.5: Contrast images showing the difference between graphene covered and uncovered parts of the MEA. The color contrast clearly shows the presence of graphene

In addition to slight film cracking observed in Pt, as mentioned in the main text, Figure A2.4 shows slight wrinkles in the bilayer graphene covering the MEA. Figure A2.5 shows SEM images taken at the edges of the graphene layer, showing a clear contrast between the graphene covered and uncovered portions of the MEA.

A Supplementary Information on Chapter 2

References

(1) Favaro, M.; Jeong, B.; Ross, P. N.; Yano, J.; Hussain, Z.; Liu, Z.; Crumlin, E. J. Unravelling the Electrochemical Double Layer by Direct Probing of the Solid/Liquid Interface. *Nat Commun* **2016**, *7*. https://doi.org/10.1038/ncomms12695.

(2) de Alwis, C.; Trought, M.; Crumlin, E. J.; Nemsak, S.; Perrine, K. A. Probing the Initial Stages of Iron Surface Corrosion: Effect of O2 and H2O on Surface Carbonation. *Appl Surf Sci* **2023**, *612*. https://doi.org/10.1016/j.apsusc.2022.155596.

(3) Dietrich, P. M.; Gehrlein, L.; Maibach, J.; Thissen, A. Probing Lithium-Ion Battery Electrolytes with Laboratory near-Ambient Pressure Xps. *Crystals (Basel)* **2020**, *10* (11), 1–13. https://doi.org/10.3390/cryst10111056.

(4) Fröhlich, N.; Fernández-Vidal, J.; Mascaró, F. V.; Shih, A. J.; Luo, M.; Koper, M. T. M. Effect of Trace Impurities in Perchloric Acid on Blank Voltammetry of Pt(111). *Electrochim Acta* **2023**, *466*. https://doi.org/10.1016/j.electacta.2023.143035.

(5) VICI AG International. *Chemical Resistance PEEK ® and Other Polymers General Reference*. https://www.daichem.co.jp/system/wp-content/themes/daichem2017/pdf/Chemical_resistance_jour.pdf. (accessed 2nd September, 2024)

(6) Saveleva, V. A.; Papaefthimiou, V.; Daletou, M. K.; Doh, W. H.; Diebold, M.; Zafeiratos, S.; Savinova, E. R.; Ulhaq-bouillet, C.; Diebold, M.; Zafeiratos, S.; Savinova, E. R. Operando Near Ambient Pressure XPS (NAP-XPS) Study of the Pt Electrochemical Oxidation in H 2 O and H 2 O/O 2 Ambients. *Journal of Physical Chemistry C* **2016**, *120* (1), 15930–15940. https://doi.org/10.1021/acs.jpcc.5b12410.

(7) Mom, R.; Frevel, L.; Velasco-Vélez, J. J.; Plodinec, M.; Knop-Gericke, A.; Schlögl, R. The Oxidation of Platinum under Wet Conditions Observed by Electrochemical X-Ray Photoelectron Spectroscopy. *J Am Chem Soc* **2019**, *141* (16), 6537–6544. https://doi.org/10.1021/jacs.8b12284.

B Supplementary Information on Chapter 3

B Supplementary Information on Chapter 3

B3.1 In situ cell sample preparation

The Polymer electrolyte membrane onto which Pt nanoparticles are to be deposited, is Nafion 117 supplied by Sigma-Aldrich. The membrane supplied by the vendor was cut into round discs of 11 mm in diameter, followed by the process of activation and cleaning. The Nafion membrane needs to be cleaned of the carbonaceous impurities. For this purpose, the Nafion discs were treated with a 3% H_2O_2 solution at 80°C for 2 hr and then with dilute H_2SO_4 solution (0.5 M) for the same duration and temperature.

The membrane electrode assembly (MEA) is prepared by sputter depositing Pt nanoparticles onto a polymer exchange membrane using a Pt target (ChemPUR GmbH, 99.5% purity) using a DC magnetron sputter coater 208HR by Cressington (Watford, UK). The process was carried out in an Argon atmosphere at 0.1 mbar and a pre-programmed sputtering current of 40 mA. The thickness of the Pt layer was controlled by automated MTM-20 high resolution thickness controller which constantly monitors the thickness of the deposited film as a function of the programmed density (for Pt = 19.45 $g.cm^{-3}$) of the material of interest and the particle deposition was calibrated using TEM. For our study, the thickness of the Pt layer was controlled between 3-4 nm.

Following the preparation of the MEA, a graphene layer is deposited on top of the Pt nanoparticles to impede the escape of the electrolyte during the spectroscopic measurements as well as to serve as an X-ray/photoelectron transparent window (>300 eV) and as the electrical contact with the Pt nanoparticles. Graphene is deposited using a wet chemical method. Graphene supported on copper (Graphenea SA) was etched in a 40 g/L solution of ammonium sulfate overnight, dissolving copper and leaving the graphene layer floating on the liquid surface which is visible against a white background. The solution was then exchanged with pure water and the MEA was placed inside the water below the graphene and the liquid level was the lowered such that the graphene layer would land on the membrane. The prepared sample with graphene was dried at room temperature and proper placement of graphene was ensured on the membrane by visual inspection.

B3.2 Change in concentration of different oxidation states of Pt with changing potential

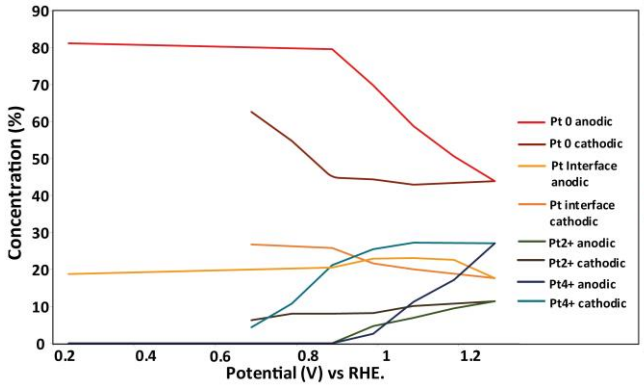

	Potential vs. RHE	Pt 0	Pt Interface	Pt 2+	Pt 4+
Anodic	0.238241	81.18	18.74	0.07	0
	0.888241	79.5	20.5	0	0
	0.988241	69.82	22.91	4.69	2.58
	1.088241	58.77	23.04	6.96	11.24
	1.188241	50.57	22.63	9.54	17.26
	1.288241	43.89	17.6	11.41	27.09
	1.388241	36.42	12.57	13.28	37.73
Cathodic	1.088241	42.92	20.05	10.22	27.25
	0.988241	44.45	21.73	8.23	25.59
	0.888241	44.91	25.77	8.09	21.23
	0.788241	54.83	26.29	8.04	10.83
	0.688241	62.65	26.74	6.25	4.34

Figure B3.1: Percentage concentration of Pt oxidation states vs applied potential

B Supplementary Information on Chapter 3

Figure B3.1 shows a detailed picture of Pt oxidation observed at different step potentials. The difference in compositions at, for example, 0.9 V_{RHE} and 1.0V_{RHE} during the cathodic and the anodic parts show the electrochemical irreversibility at which the oxide species on platinum are formed and reduced.

B3.3 Catalyst wetting observed via XAS spectrum

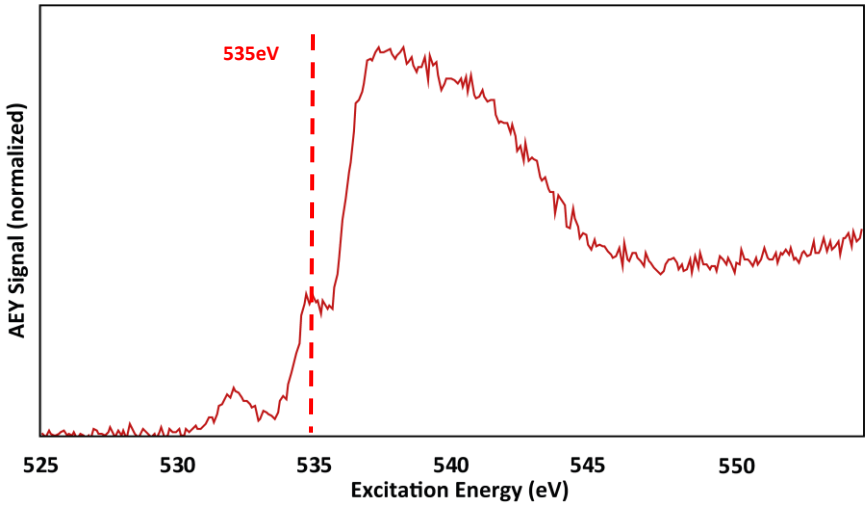

Figure B3.2: Effect of graphene covering on O-K edge spectra recorded at 0.7 V_{RHE}

One of the most important features of the in situ spectroscopy cell is its ability to ensure the wettability of the catalyst under vacuum conditions. To check the wetting of the catalyst, we use in situ O-K-edge XAS spectroscopy, which is conducted during the in situ XPS experiments in the same geometry. One of the most important features in the O-K-edge spectrum that we have used to track the wetting of the Pt nanoparticles is the peak at 535 eV, which is very typical for liquid water[1,2]. The O-K edge spectrum shown in Figure B3.2 is measured at a low potential of 0.7 V_{RHE} to avoid the contribution from platinum oxides. To reduce the noise in the PEY spectrum, an average of several spectra was taken at several locations on the catalyst surface to avoid the effects of beam damage.

As shown in Figure B3.2, the 535 eV peak is very pronounced. This can only be explained by either the presence of liquid water, or by a significant contribution from graphene oxide to the spectrum. However, graphene oxide also produces a strong resonance at about 531.9 eV. In our case, only a weak contribution is visible, ruling out the possibility that functional groups on the graphene window have contributed significantly to the 535 eV peak[1]. Hence, we can say with certainty that the peak at 535 eV in the O-K edge spectrum predominantly originates from water, i.e. that the catalyst layer was properly wetted during the in situ XPS experiments.

B Supplementary Information on Chapter 3

B3.4 XPS Data fitting parameters

The raw XPS data was processed using CasaXPS Version 2.3.23. A Shirly background subtraction was used for all the datasets. The Lorentzian LF line shape was employed, which is an extension of Lorentzian LA line shape, the purpose of which is to limit the intensity of the asymmetric tails. It fits the data on the basis of 4 parameters;α, β, w and m. Varying 'α' and 'β' results in increasing or decreasing the spread of the tail for the Lorentzian curve, thereby affecting how steep are the edges of the line shape. 'm' is the integer specifying the Lorentzian convolution by the gaussian function and 'w' is the dampening factor to force the tails of the curve to reduce towards the limits of integration. An asymmetric form of Lorentzian LF line shape function was used for fitting the raw Pt4f spectra. It is known through literature that, as a consequence of spin-orbit coupling, the electrons that leave Pt4f orbital, generate two distinct energy peaks in the XPS spectrum categorized as $4f_{5/2}$ and $4f_{7/2}$. Hence doublets for Pt^0 $Pt^{\delta+}$, Pt^{2+} and Pt^{4+} were used, with a constant spin-orbit splitting of 3.34 eV and a peak area ratio of 3:4 for the $4f_{5/2}$ and $4f_{7/2}$ peaks. The details of the fitting parameters are shown in the table below.

	Pt^0	**$Pt^{\delta+}$**	**Pt^{2+}**	**Pt^{4+}**
Line shape	LF(0.63,2,20,70)	LF(0.63,2,20,70)	LF(0.63,2,20,70)	LF(1.8,2,10,0)
Peak Position	70.81 - 70.7999	72 - 71.2	72.7 - 72	Determined at highest potential of the dataset
FWHM	Free	Same as Pt0	Same as Pt0	Determined at highest potential of the dataset

Table C3.1: Fitting parameters for Pt 4f spectral decomposition

The ranges for the peak positions of different Pt oxidation states were determined in accordance with the literature, especially cited in detail by Savelena and their group[3] and previous work [1]. In order to accommodate the variations in the configuration of the beam energy for different experiments, a slight variation in the binding energy for Pt^0 (± 0.1 eV) was permitted. The line shape parameters were determined in similar fashion as in previous work [1]. The Pt^{4+} line shape, peak position, and FWHM were determined by free fitting of a highly oxidized 4nm Pt sample produced at 1.85 V_{RHE}, which displays a well-resolved Pt^{4+} peak. The line shape and FWHM of the other components was determined at low potential, where the metallic contribution is dominant. Note, however, that there is no potential at which only one component could be fitted. This is in line with the notion that the Pt surface atom are always in contact with adsorbates (e.g. H_2O, OH, O, R-SO_3^-), which generates a $Pt^{\delta+}$ and a bulk Pt^0 peak. The consistency of the fit model was ensured by applying it to several data sets.

B Supplementary Information on Chapter 3

B3.5 Charge transfer calculation for XPS data

As mentioned in the main text, an oxidation charge transfer value was calculated based on the ratio of oxidation states observed in the XPS data. Since the comparison of this value is to be drawn with the measured surface oxidation charge of Pt nanoparticles in the electrochemical cell, the XPS data (as shown in Figure B3.1) had to be corrected to represent the surface of the nanoparticle only. To estimate the fraction of the total XPS signal emerging from the nanoparticle surface, it was assumed that at 1.4 V_{RHE} the surface layer is completely oxidized (as confirmed by oxide layer thickness modelling). Hence, the signal from Pt^0 at 1.4 V_{RHE} arises from subsurface while $Pt^{\delta+}$, Pt^{2+} and Pt^{4+} species constitute the surface signal, which comes out to be ~63% of the measured XPS signal. The intensities of the $Pt^{\delta+}$, Pt^{2+} and Pt^{4+} contributions shown in Figure B3.1 were rescaled using this number, so that they represent the fraction of the surface that was occupied by these species.

The basis of oxidation charge calculation is the formation of a monolayer of oxides on the Pt surface and considering the formation of PtO(Pt^{2+}), PtO_2(Pt^{4+}) and $Pt_{Interface\ oxide}$($Pt^{\delta+}$) as $2e^-$, $4e^-$ and $1e^-$ transfer processes, respectively. The average no. of e- transferred by the surface Pt atoms was calculated for each value of the step potentials shown in Figure B3.1 as follows:

$$Avg.e-transferred = \frac{(x_{Pt\,\delta+}*1)+(x_{Pt\,2+}*2)+(x_{Pt\,4+}*4)}{0.63} \quad (2)$$

Where $x_{Pt\,i}$ is the measured fraction of Pt species and 0.63 represents the fraction of the XPS signal originating from the surface of the nanoparticle. The calculated average number of electrons transferred has to be corrected to exclude the contribution from adsorbed oxygen or OH species (O_{ads}/OH_{ads}) that are already present at the base potential of the pulses in the electrochemical experiment (0.7 V_{RHE}). We approximated this correction by subtracting the number of electrons transferred at 0.9 V_{RHE} from the ones calculated at higher potentials:

$$Corrected\ e-transferred\ at\ V_{pulse} = \left(Calculated\ e-transferred\ at\ V_{pulse}\right) - (e-transfred\ at\ 0.9\ V_{RHE}) \quad (3)$$

Where $V_{pulse} = 1.2, 1.3\ and\ 1.4\ V_{RHE}$.

B Supplementary Information on Chapter 3

B3.6 XAS experiments with consecutive voltage pulses

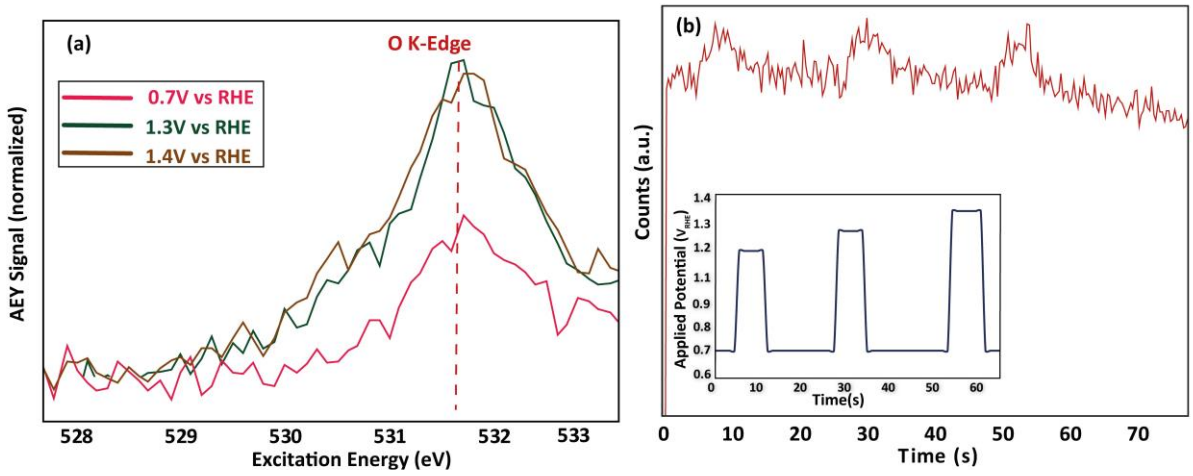

Figure B3.3: XAS spectra for applied pulse potentials. (a) Inset shows the consecutive pulses applied and the main set shows tracked XAS spectrum peak at 531.9 eV while (b) shows the same peak at different pulse potential in overlay arrangement

Figure B3.3(a) shows XAS spectra tracking the O K-edge peaks at 531.9 eV, which is associated with the formation of Pt oxides[1] exhibiting significant oxidation at higher anodic potentials. It is also indicated in the literature that a high O K-edge intensity between 529.5 eV and 532 eV at potentials as high as 1.3 V_{RHE} and 1.4 V_{RHE} can be associated with the formation of a considerable amount of PtO_2[4–6] which is consistent with our XPS results. The O K-edge spectrum in the main set of Figure B3.3(b) show a corresponding sharp spike at 531.9 eV for every potential pulse applied as shown in the inset, indicating significant oxidation during SU/SD pulses. It is also noticeable that for each of these pulse responses, the rise is much steeper than the fall which tells us about the kinetics of oxidation (rise) being much faster than reduction (fall).

B3.7 Extended potential pulse experiment (XAS)

To observe the oxidation behavior for prolonged oxide conditioning times, the applied potential was raised instantaneously from 0.7 V_{RHE} and to 1.4 V_{RHE} and maintained, with the intensity of the O-K edge at 531.9 eV tracked as a function of time. It can be seen clearly from Figure B3.4 that the O-K edge peak shows a plateau following an instantaneous spike in counts as a function of potential pulse, indicating swift surface oxidation of Pt nanoparticles after which the role of diffusion becomes more important and oxidation slows down. This observation confirms the conclusion that was drawn from similar electrochemical experiment indicated in Figure 3.6.

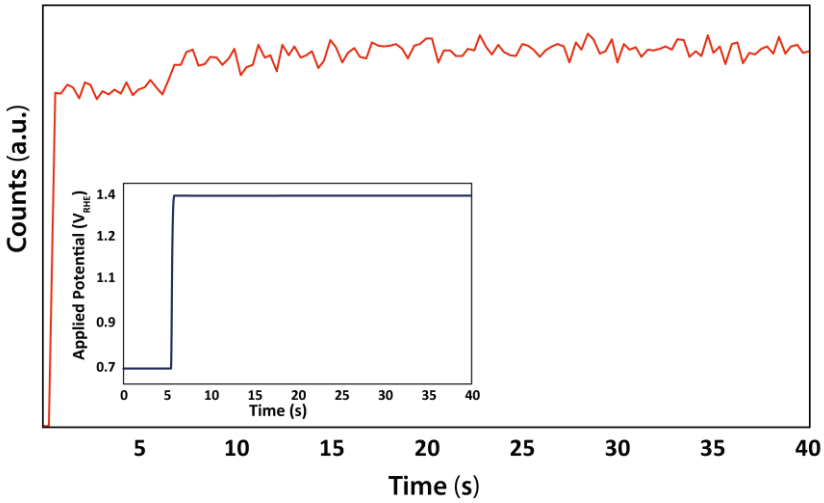

Figure B3.4:Time resolved O-K edge peak intensity at 531.9 eV (main set) for potential hold scheme at 1.4 V_{RHE} (inset)

B3.8 Modelling of oxide layer thickness

The initial particle size before oxidation was taken as 2.5 nm. All the components highlighted in the XPS data fitting (see Figure 3.4) were incorporated in the thickness modelling for both the models discussed below.

a) Shard's model

Shard's model[7] provides us with a straightforward approach to estimate the thickness of the overlayer on a nanoparticle as a function of the normalized XPS intensities observed experimentally. In our paper, the fundamental equation adopted from the Shard's model to estimate the oxide layer thickness is as follows;

$$T_{NP} = \frac{T_{R\sim1} + \beta T_o}{1+\beta} \tag{4}$$

Where T_{NP} is the thickness of the oxide layer, while $T_{R\sim1}$, β and T_o are variables which are calculated as a function of α, β and core radius of the nanoparticle (R). α and β are calculated as follows:

$$\alpha = \frac{1.8}{A^{0.1}B^{0.5}C^{0.4}} \tag{5}$$

$$\beta = \frac{0.13\alpha^{2.5}}{R^{1.5}} \tag{6}$$

Based on previous TEM data[1], we estimate the core radius to be around 2.5 nm for unoxidized particles.

Shard's model in essence takes into account one[1] component in the core of the particle and one component in the oxide shell. For our model, a weighted average of the relative electron attenuation length and normalized XPS intensities had to be incorporated into variables A and C to take into account all the oxide components identified in the XPS analysis:

$$A = \left(\left(\frac{x_{Pt\,\delta+}}{x_{Pt\,\delta+}+x_{Pt\,2+}+x_{Pt\,4+}}\right)\left(\frac{I_{Pt\,\delta+}}{I_{Pt}}\right)\left(\frac{I^{o}_{Pt}}{I^{o}_{Pt\,\delta+}}\right)\right) + \left(\left(\frac{x_{Pt\,2+}}{x_{Pt\,\delta+}+x_{Pt\,2+}+x_{Pt\,4+}}\right)\left(\frac{I_{Pt\,2+}}{I_{Pt}}\right)\left(\frac{I^{o}_{Pt}}{I^{o}_{Pt\,2+}}\right)\right) + \left(\left(\frac{x_{Pt\,4+}}{x_{Pt\,\delta+}+x_{Pt\,2+}+x_{Pt\,4+}}\right)\left(\frac{I_{Pt\,4+}}{I_{Pt}}\right)\left(\frac{I^{o}_{Pt}}{I^{o}_{Pt\,4+}}\right)\right) \quad (7)$$

$$C = \left(\left(\frac{x_{Pt\,\delta+}}{x_{Pt\,\delta+}+x_{Pt\,2+}+x_{Pt\,4+}}\right)\left(\frac{L_{Pt\,\delta+}}{L_{Pt}}\right)\right) + \left(\left(\frac{x_{Pt\,2+}}{x_{Pt\,\delta+}+x_{Pt\,2+}+x_{Pt\,4+}}\right)\left(\frac{L_{Pt\,2+}}{L_{\,Pt}}\right)\right) + \left(\left(\frac{x_{Pt\,4+}}{x_{Pt\,\delta+}+x_{Pt\,2+}+x_{Pt\,4+}}\right)\left(\frac{L_{Pt\,4+}}{L_{Pt}}\right)\right) \quad (8)$$

where

$x_{Pt\,i}$ (where i= $\delta+, 2+, 4+$) : concentration of $Pt^{\delta+}$, Pt^{2+} and Pt^{4+}

$\frac{I_{Pt\,i}}{I_{Pt}}$ = ratio of measured XPS intensity of oxide component i in the shell and metallic Pt (assumed to be) in the core

$\frac{L_{Pt\,i}}{L_{Pt}}$ = ratio of the attenuation length of the photoelectrons arising from material i when travelling in the shell to the attenuation length of the photoelectrons arising from material i when traveling in the core

$\frac{I^{o}_{Pt}}{I^{o}_{Pt\,i}}$ = ratio of XPS intensities for a flat, pure Pt metal surface and a flat pure version of material i.

B is the ratio of attenuation lengths of the core and shell material for photoelectrons traveling in the shell. Since the kinetic energy of the photoelectrons of all species discussed here is roughly the same, B can be taken as 1.

The pure component intensities are estimated in this model using the following expression;

$$\frac{I^{o}_{Pt}}{I^{o}_{Pt\,i}} = \frac{N^{o}_{Pt}.L_{PtinPt}.G(E_{Pt})}{N^{o}_{Pt\,i}.L_{\,i\,in\,i}.G(E_{Pt\,i})} \quad (9)$$

In the above equation, N^{o}_{Pt} and $N^{o}_{Pt\,i}$ are the number densities (g.cm^{-3}) of pure metal and pure oxide components (Pt= 21.45, $Pt^{\delta+}$($Pt_{\text{interface oxides}}$)= 20, Pt^{2+}(PtO)= 14.9, Pt^{4+}(PtO_2)= 10.2), L_{PtinPt} is the attenuation length in pure metallic Pt, $L_{\,i\,in\,i}$ is the attenuation length in material i, and $G(E_{Pt})$and $G(E_{Pt\,i})$ are the spectrometer transmission factors as a function of photoelectron kinetic energies. Since the kinetic energy of the photoelectrons of all species discussed here is roughly the same, the transmission factors are taken as equal and cancel out.

Note that the shell thickness T and the particle radius R are expressed in units of $L_{Pt\,i}$ in the model.

B3.8 Ertl and Küpper's model

Ertl and Küpper's model is an alternative way to estimate the oxide layer thickness (d) on the nanoparticles[8]. The equation used in the modelling of the thickness is as follows;

B Supplementary Information on Chapter 3

$$d = L_{avg}.cos\theta.ln\left(1+\frac{I_{ox}.I_M^o}{I_M.I_{ox}^o}\right) \quad (10)$$

Where L_{avg} stands for the average photoelectron attenuation length based on the weighted average of the metal and oxide species (done similarly as in Shard's model), θ is the take-off angle normal to the surface (taken as 57° here). The value of take-off angle is derived from the publication of Castner and coworkers, who have used similar values for nanoparticles of a comparable size as our application[9].

B Supplementary Information on Chapter 3

References

(1) Mom, R.; Frevel, L.; Velasco-Vélez, J. J.; Plodinec, M.; Knop-Gericke, A.; Schlögl, R. The Oxidation of Platinum under Wet Conditions Observed by Electrochemical X-Ray Photoelectron Spectroscopy. *J. Am. Chem. Soc.* **2019**, *141* (16), 6537–6544. https://doi.org/10.1021/jacs.8b12284.

(2) Merte, L. R.; Behafarid, F.; Miller, D. J.; Friebel, D.; Cho, S.; Mbuga, F.; Sokaras, D.; Alonso-mori, R.; Weng, T. C.; Nordlund, D.; Nilsson, A.; Cuenya, B. R.; Roldan Cuenya, B. Electrochemical Oxidation of Size-Selected Pt Nanoparticles Studied Using in Situ High-Energy-Resolution X - Ray Absorption Spectroscopy. *ACS Catal.* **2012**, *2* (11), 2371–2376. https://doi.org/10.1021/cs300494f.

(3) Saveleva, V. A.; Papaefthimiou, V.; Daletou, M. K.; Doh, W. H.; Diebold, M.; Zafeiratos, S.; Savinova, E. R.; Ulhaq-bouillet, C.; Diebold, M.; Zafeiratos, S.; Savinova, E. R. Operando Near Ambient Pressure XPS (NAP-XPS) Study of the Pt Electrochemical Oxidation in H 2 O and H 2 O/O 2 Ambients. *J. Phys. Chem. C* **2016**, *120* (1), 15930–15940. https://doi.org/10.1021/acs.jpcc.5b12410.

(4) Kaya, S.; Casalongue, H. S.; Friebel, D.; Anniyev, T.; Miller, D. J. Oxidation of Pt (111) under Near-Ambient Conditions. **2011**, *195502* (November), 1–5. https://doi.org/10.1103/PhysRevLett.107.195502.

(5) Costa, D.; Dintzer, T.; Arrigo, R.; Knop-gericke, D. A. Chemical Science In Situ Investigation of Dissociation and Migration Phenomena at the Pt / Electrolyte Interface of An. **2015**, 5635–5642. https://doi.org/10.1039/C5SC01421B.

(6) H.Yoshida, S. Nonoyama, Y. Yazawa, T. H. Quantitative Determination of Platinum Oxidation State by XANES Analysis. *Phys. Scr. T* **2005**, *115* (1), 813–815. https://doi.org/https://doi.org/10.1238/Physica.Topical.115a00813.

(7) Shard, A. G. A Straightforward Method for Interpreting XPS Data from Core-Shell Nanoparticles. *J. Phys. Chem. C* **2012**, *116* (31), 16806–16813. https://doi.org/10.1021/jp305267d.

(8) Ertl, G., Küppers, J., & Grasserbauer, M. Low Energy Electrons and Surface Chemistry. *Anal. Chim. Acta* **1987**, *199* (1), 272–273. https://doi.org/https://doi.org/10.1016/s0003-2670(00)82831-7.

(9) Techane, S. D.; Gamble, L. J.; Castner, D. G. Multitechnique Characterization of Self-Assembled Carboxylic Acid-Terminated Alkanethiol Monolayers on Nanoparticle and Flat Gold Surfaces. **2011**, 9432–9441.

C Supplementary Information on Chapter 4

C Supplementary Information on Chapter 4

C4.1 Nafion Membrane Activation

The Polymer electrolyte membrane with sputtered Pt nanoparticles is Nafion 117 supplied by Sigma-Aldrich. The membrane was cut into 1 cm squares, followed by the process of activation and cleaning. The Nafion membrane needs to be cleaned of the carbonaceous impurities. For this purpose, the samples were treated with a 3% H_2O_2 solution at 80^oC for 2 hr and then with dilute H_2SO_4 solution (0.5 M) for the same duration and at the same temperature. Following the cleaning procedure, the membranes were rinsed with deionized water and stored dry.

C4.2 Glassy Carbon (GC) electrode preparation

5 mm diameter GC discs were polished with polycrystalline diamond suspension (MetaDi^{TM} Supreme, Buehler) to a mirror finish. The electrodes were then ultrasonicated in deionized water to remove polishing solution residue. Clean GC discs were dried in an Argon gas stream. Pt and Pt_3Ni nanoparticles were sputter deposited onto the cleaned discs.

C4.3 Membrane Electrode Assembly Preparation

Pt_3Ni alloy and Pt metal were used to prepare the membrane electrode assembly (MEA) by sputter depositing the catalyst nanoparticles onto activated Nafion 117 polymer exchange membranes.

For Pt MEA samples, a Pt target (ChemPUR GmbH, 99.5% purity) and a DC magnetron sputter coater 208HR by Cressington (Watford, UK), were employed. A sputtering current of 40 mA was used with the sputter chamber pressure maintained at ~$4x10^{-4}$ Pa. The sputtering process lasted for 2 minutes and 45 seconds to deposit a 5 nm thick layer of Pt.

Pt_3Ni alloys were deposited using two circular TORUS magnetrons (Kurt J. Lesker) operating simultaneously. 2" Pt (99.99% Safina) and 2" Ni (99.99% Kurt J. Lesker) targets were employed for the sputtering of Pt and Ni, respectively. Prior to deposition, the sputtering chamber was evacuated to a base pressure of 1×10^{-4} Pa. Sputtering was then performed in a 2.6 Pa argon atmosphere in DC mode, with the power set to 28 W for Pt and 30 W for Ni to achieve the desired alloy composition. The deposition lasted for 1 minute and 35 seconds to attain a 5 nm thickness of the deposited layer.

C4.4 Graphene deposition on the Nafion MEA

Following the preparation of the MEA, a graphene bi-layer is deposited on top of the Pt nanoparticles to impede the escape of the electrolyte during the spectroscopic measurements in the XPS vacuum chamber. This graphene serves as both an X-ray/photoelectron transparent window (>300 eV) and as the electrical contact with the Pt nanoparticles. Graphene is deposited using a wet chemical method. For this purpose, graphene supported on copper (Graphenea SA) was etched in a 40 g/L solution of ammonium persulfate overnight, dissolving copper and leaving the graphene layer floating on the liquid surface. The solution was then exchanged with pure water and the floating graphene was scooped off the surface of the water with the MEA. The prepared sample with graphene was dried at room temperature and proper placement of graphene was ensured on the membrane by visual inspection.

C4.5 EDX Sample Analysis

The sample composition was verified through bulk-sensitive Energy-Dispersive X-ray Spectroscopy (EDX), utilizing an XFlash detector (Bruker) integrated into the Mira 3 Scanning electron microscope (Tescan) operated at electron energy of 30 keV.

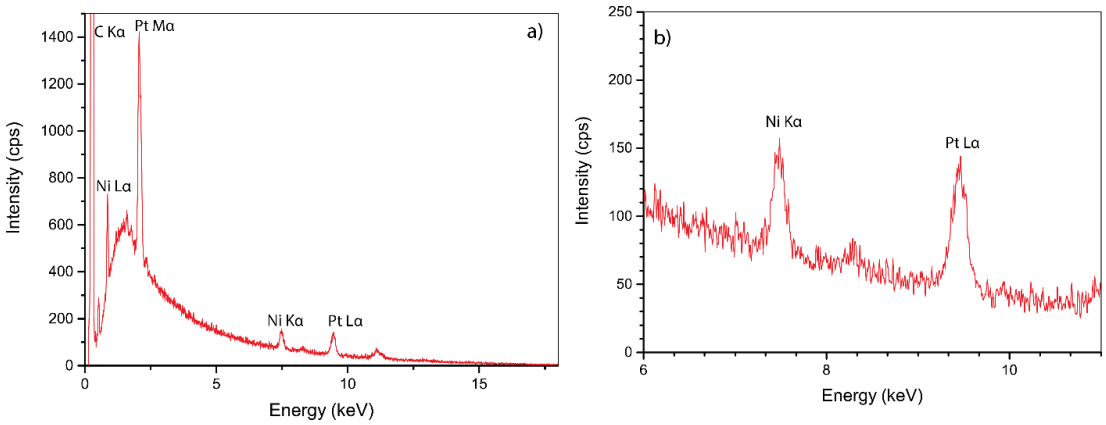

Figure C4.1: Energy Dispersive X-ray (EDX) analysis of as-prepared Pt_3Ni samples

The bulk composition of the as-deposited Pt_3Ni layer was quantified from the EDX spectra shown in Figure C4.1 by integrating the Ni $K\alpha_1$ (7.480 keV) and Pt $L\alpha_1$ (9,442 keV) lines. The calculated composition was $Pt_{73}Ni_{27}$, close to the intended Pt_3Ni composition.

C4.6 Cell Design

All experiments were performed in the newly designed Spectro-electrochemical flow-cell shown in Figure C4.2. A titanium top plate secures the MEA in the cell. A Pt wire is used as a counter electrode and Ag/AgCl electrode is used as a reference. Electrolyte connections are present at the rear of the cell, to which the electrolyte lines are connected via PTFE fittings. The main body of the cell is made out of PEEK. The cross section of the cell shown on the right hand side in Figure C4.2 shows the internal electrolyte cavity and the circulation. A minimum dead volume is maintained inside the cavity, minimizing the distance between the electrodes and the cell resistance.

C Supplementary Information on Chapter 4

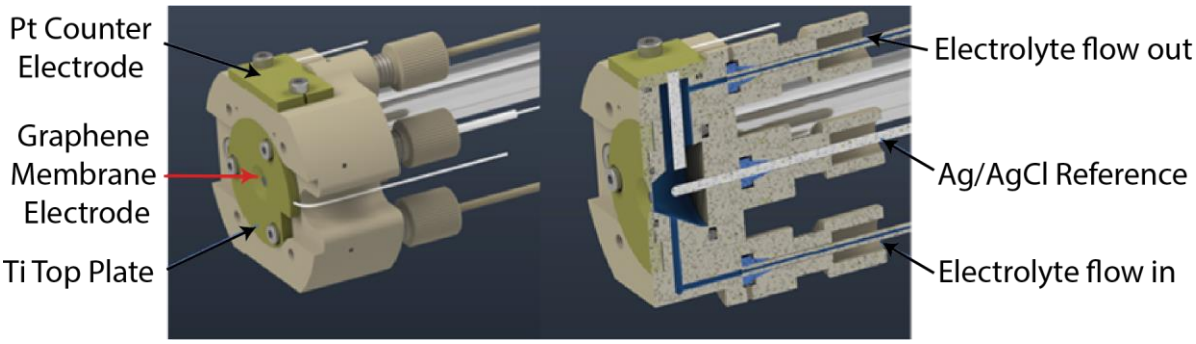

Figure C4.2: Schematic of the three-electrode spectro-electrochemical cell set-up for in-situ X-ray spectroscopy.

C4.7 Pt 4f XPS Data fitting

The raw XPS data was processed using CasaXPS Version 2.3.23. A Tougaard background subtraction was used for all the datasets. The Lorentzian LF line shape was employed, which is an extension of the Lorentzian LA line shape, the purpose of which is to limit the intensity of the asymmetric tails. It fits the data on the basis of 4 parameters;α, β, w and m. Varying 'α' and 'β' results in increasing or decreasing the spread of the tail for the Lorentzian curve, thereby affecting the steepness of the edges of the line shape. 'm' is the integer specifying the Gaussian convolution with the Lorentzian function and 'w' is the dampening factor to force the tails of to zero towards the limits of integration. An asymmetric form of Lorentzian LF line shape function was used for fitting the raw Pt 4f spectra. Doublets for Pt^0 $Pt^{\delta+}$, Pt^{2+} and Pt^{4+} were used, with a constant spin-orbit splitting of 3.34 eV and a peak area ratio of 3:4 for the $4f_{5/2}$ and $4f_{7/2}$ peaks. The details of the fitting parameters are shown in the table below.

The ranges for the peak positions of different Pt oxidation states were determined in accordance with the literature, as summarized by Saveleva *et al.*[1], and previous work[2]. In order to accommodate the variations in the configuration of the beam energy for different experiments, a slight variation in the binding energy for Pt^0 (± 0.1 eV) was permitted. The Pt^{4+} line shape, peak position, and FWHM were determined by free fitting of a highly oxidized 5nm Pt sample produced at 1.7 V_{RHE}, which displays a well-resolved Pt^{4+} peak. The line shape and FWHM of the other components was determined at low potential, where the metallic contribution is dominant. Note, however, that there is no potential at which only one component could be fitted. This is in line with the notion that the Pt surface atom are always in contact with adsorbates (e.g. H_2O, OH, O, R-SO_3^-), which generates a $Pt^{\delta+}$ and a bulk Pt^0 peak. The consistency of the fit model was ensured by applying it to several data sets.

C Supplementary Information on Chapter 4

	Pt^0	$Pt^{\delta+}$	Pt^{2+}	Pt^{4+}
Line shape	LF(0.9,2,60,50)	LF(0.9,2,60,50)	LF(0.9,2,60,50)	LF(3,3,30,10)
Peak Position	71.2 - 70.9	72 - 71.2	72.7 - 72	Determined at highest potential of the dataset
FWHM	Free	Same as Pt^0	Same as Pt^0	Determined at highest potential of the dataset

Table C4.1 : Fitting parameters for Pt 4f spectral decomposition

C4.8 Pt 4f / Ni 2p peak area integration

Pt 4*f* spectra were recorded at 600 eV excitation energy with 10 eV pass energy while the Ni 2*p* spectra were measured at 1900 eV excitation energy with 50 eV pass energy at same measurement spot. A different measurement spot was chosen for every potential to avoid beam damage to the Nafion membrane. A Tougaard background subtraction was applied to the spectra and the area under the curve was integrated in CasaXPS. The Pt 4*f* / Ni 2*p* ratio was calculated by simply dividing the area under the Pt 4*f* and Ni 2*p* spectra.

C4.9 Pt_3Ni SEM Images

Figure C4.3 shows the SEM images taken for an 'as prepared' Pt_3Ni MEA sample. A clear contrast between the graphene covered (dark) and bare catalyst surface (bright) on the MEA can be seen in Figure C4.3a by imaging at the edge of the deposited graphene. An area in the middle the graphene window is shown in Figure C4.3b. The lack of microscopic tears in the graphene confirms the quality of the window. Figure C4.3c shows a higher magnification. Here, the contrast originates from the catalyst layer (light) with respect to the non-conductive underlying Nafion (dark), both of which are imaged through the (fairly) electron-transparent graphene window. A clear cracking pattern can be observed, which is formed when the Pt_3Ni-coated Nafion membrane is inserted in water to pick up the graphene window. Nafion swells by about 10% in water, cracking up the film.

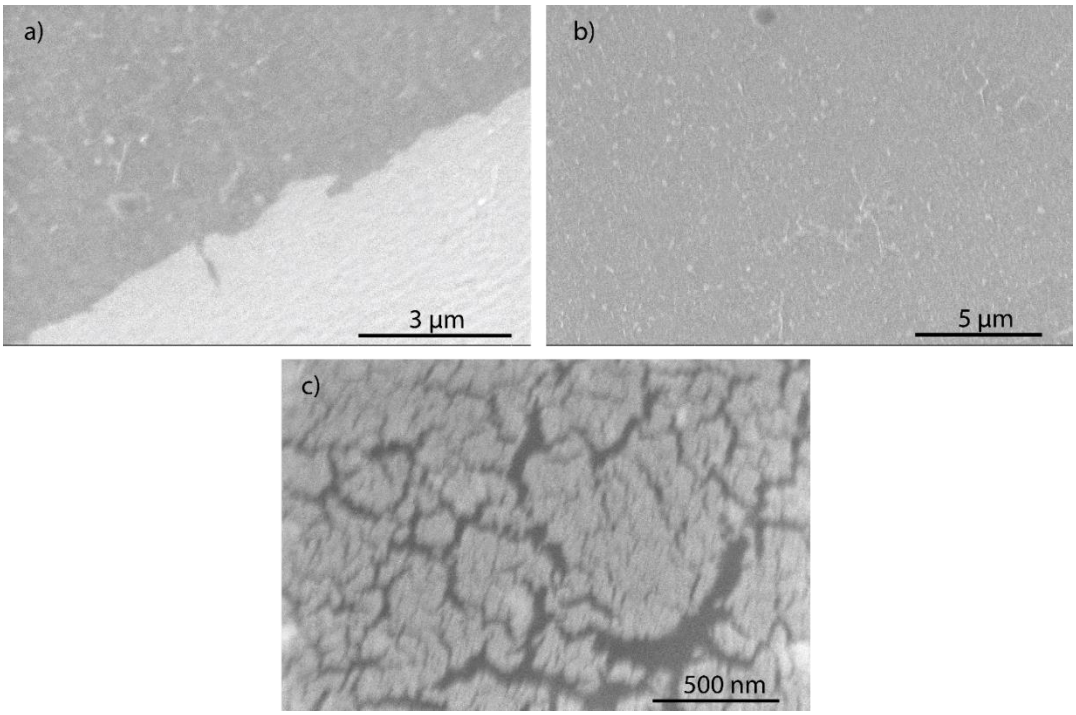

Figure C4.3: SEM Images for Pt_3Ni catalyst sputter deposited onto cleaned and activated Nafion membrane

Unfortunately, attaining higher resolution images of the MEA was not possible due to charging and beam damage of the Nafion membrane. However, Figure C4.4 shows a collection of SEM images for a similar catalyst loading deposited on a polished glassy carbon surface. Clusters of aggregated catalyst particles can be seen, with a grain size of about 8 nm.

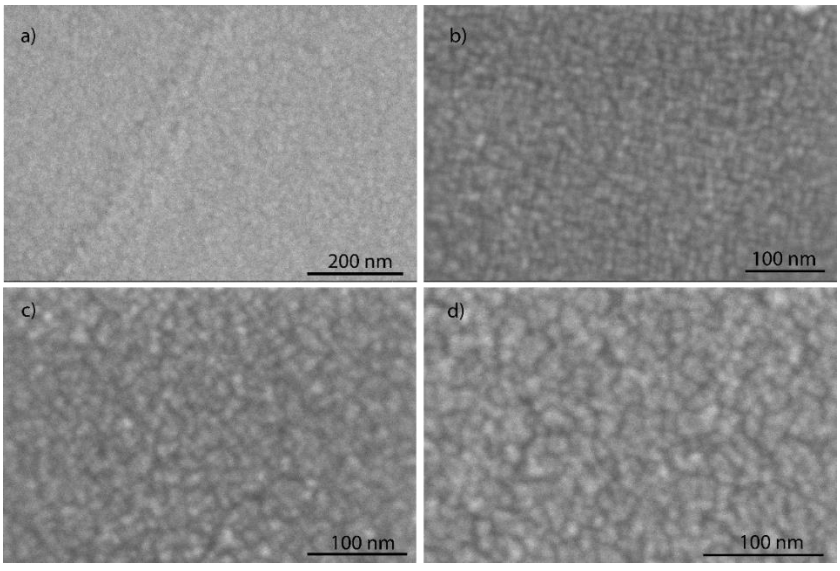

Figure C4.4: SEM Images for Pt_3Ni catalyst sputter deposited onto polished glassy carbon disk

C4.10 XAS Data processing and arctan correction for Ni L3 edge

Ni L-edge XAS data was processed using Athena (version 0.9.26), applying a linear pre-and post-edge correction and a normalization to the edge jump. The correctness of the processing was verified using the L_2-edge jump, which should be 0.5 for a spectrum normalized to the L_3

edge jump due the spin-orbit splitting ratio of the 2p core level. In addition, we checked that the L_2 edge whiteline intensities showed the same trends as the L_3-edge whiteline intensity.

For the analysis of the intensity and weighted average peak position of the Ni L_3-edge in Figure 4.4 in the Main Text, an arctan baseline subtraction was applied using OriginPro 2017. Figure C4.5a (red curve) shows an example. The resultant background corrected curve is shown in Figure C4.5b, whereas Figure C4.5c shows its integrated version. The dotted lines in Figure C4.5c coincide with the middle (half) of the integrated intensity on the *y*-axis. The corresponding photon energy was used as the weighted average peak position in Figure C4.5c. For the peak intensity in Figure C4.4b of the Main Text, the plateau value of the integral was used, i.e. the area under the arctan baseline subtracted peak.

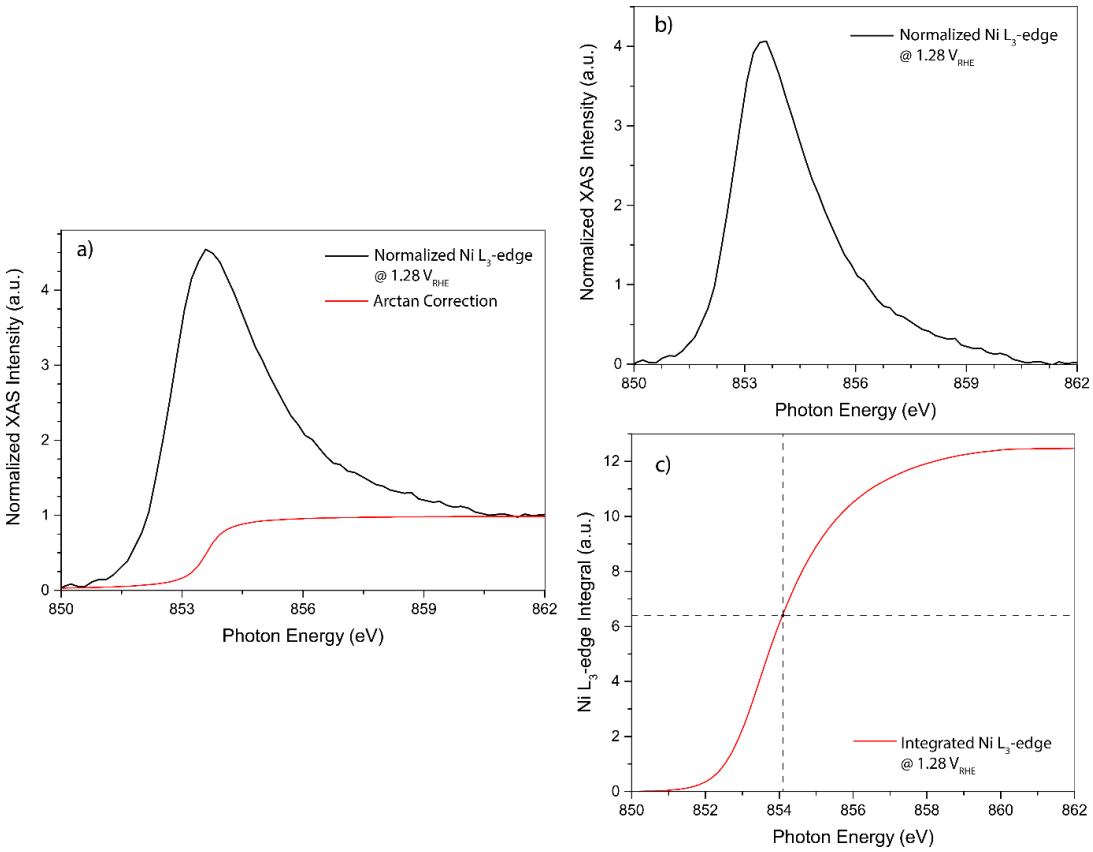

Figure C4.5: Arctan correction for the analysis of the Ni L_3-edge spectra; a) shows an example spectrum (black curve) and an arctan function to be subtracted (red curve), b) shows the resultant curve after the subtraction and c) shows the integrated version of b), where the dotted line indicated the weighted average peak position on the x-axis

C4.11 Pt & Pt_3Ni Cyclic voltammogram and activity

Pt and Pt_3Ni catalysts were tested in a glass cell for their electrochemical behavior measured in Argon purged 0.1 M H_2SO_4. Figure C4.6 shows similar voltametric behavior in the glass cell as observed in the spectro-electrochemical experiments discussed in the main text (Figure 4.1b), where weak adsorbate interaction in Pt_3Ni, as well as higher oxidation current as compared to bulk Pt catalyst, can be observed.

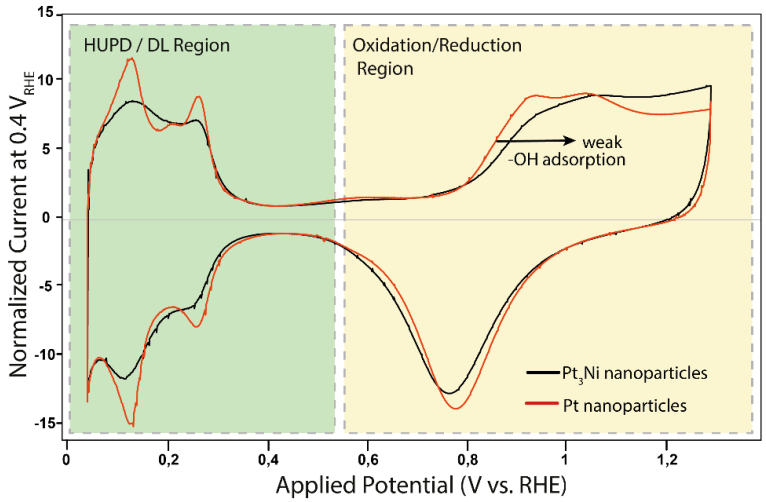

Figure C4.6: Cyclic voltammograms of Pt and Pt_3Ni catalyst nanoparticles deposited on glassy carbon substrate in Ar purged 0.1M H_2SO_4 highlighting Hydrogen Underpotential Deposition (HUPD), Double Layer (DL) and oxidation/reduction regions

C4.12 Ni 2p potential dependent XPS Spectra

Figure C4.7 shows Ni 2*p* XPS spectra measured at different potentials. The binding energy is consistent with metallic Ni.

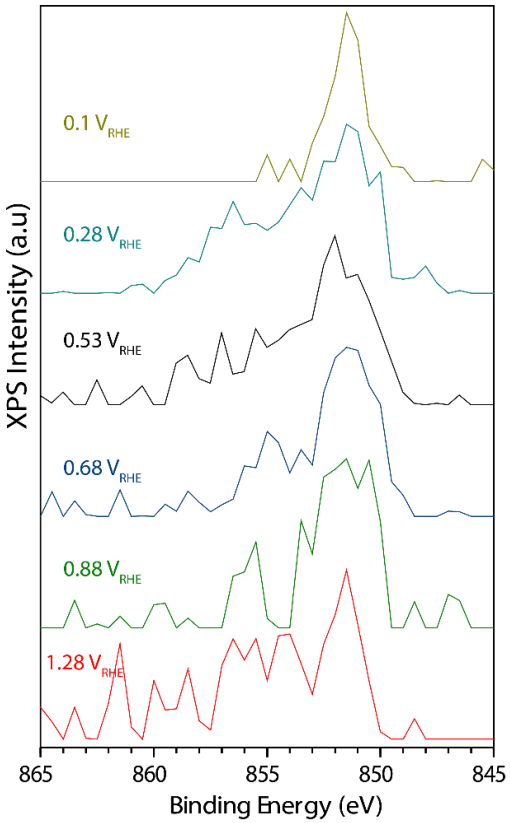

Figure C4.7: Ni 2p XPS spectra as a function of potential at 1900 eV excitation energy

C Supplementary Information on Chapter 4

References

(1) Saveleva, V. A.; Papaefthimiou, V.; Daletou, M. K.; Doh, W. H.; Diebold, M.; Zafeiratos, S.; Savinova, E. R.; Ulhaq-bouillet, C.; Diebold, M.; Zafeiratos, S.; Savinova, E. R. Operando Near Ambient Pressure XPS (NAP-XPS) Study of the Pt Electrochemical Oxidation in H 2 O and H 2 O/O 2 Ambients. *Journal of Physical Chemistry C* 2016, *120* (1), 15930–15940. https://doi.org/10.1021/acs.jpcc.5b12410.

(2) Javed, H.; Knop-Gericke, A.; Mom, R. V. Structural Model for Transient Pt Oxidation during Fuel Cell Start-up Using Electrochemical X-Ray Photoelectron Spectroscopy. *ACS Appl Mater Interfaces* 2022, *14* (31), 36238–36245. https://doi.org/10.1021/acsami.2c09249.